Low Temperature Physics/Fizika Nizkikh Temperatur, 2016, v. 42, No. 7, pp. 710–715

Electronic structure of cubic ScF_3 from first-principles calculations

D. Bocharov[1], P. Žguns[1,2], S. Piskunov[1], A. Kuzmin[1], and J. Purans[1]

[1]*Institute of Solid State Physics, University of Latvia, 8 Kengaraga Str., LV-1063 Riga, Latvia*
E-mail: bocharov@latnet.lv

[2]*Department of Physics and Astronomy, Uppsala University, Uppsala 75121, Sweden*

Received February 22, 2016, published online May 25, 2016

The ground state properties of cubic scandium trifluoride (ScF_3) perovskite were studied using first-principles calculations. The electronic structure of ScF_3 was determined by linear combination of atomic orbital (LCAO) and plane wave projector augmented-wave (PAW) methods using modified hybrid exchange-correlation functionals within the density functional theory (DFT). The comprehensive comparison of the results obtained by two methods is presented. Both methods allowed us to reproduce the lattice constant found experimentally in ScF_3 at low temperatures and to predict its electronic structure in good agreement with known experimental valence-band photoelectron and F 1*s* x-ray absorption spectra.

PACS: 71.20.Ps Other inorganic compounds;
71.15.Ap Basis sets (LCAO, plane-wave, APW, etc.) and related methodology (scattering methods, ASA, linearized methods, etc.).

Keywords: scandium fluorite, first-principles calculations, density functional theory, electronic structure, negative thermal expansion.

Introduction

Scandium trifluoride (ScF_3) is a promising material attracted much attention due to its crystal lattice experiences strong negative thermal expansion (NTE) when temperature increases from 10 to 1100 K [1]. At atmospheric pressure ScF_3 has cubic (space group *Pm*-3*m* (221)) ReO_3-type structure (Fig. 1) down to at least 10 K [1]. However, opposite to the metallic ReO_3, which has very week NTE effect [2–4], scandium trifluoride is an insulator with band gap of more than 8 eV [5].

The cubic ReO_3 structure type is often used as a simple illustration of how negative thermal expansion can arise from the thermally induced rocking of rigid unit mode [6,7]. The ionic character, cubic structure and very pronounced NTE of ScF_3 made this compound attracting object for experimental studies [8–11] as well as a interesting object for modelling. Moreover, other interesting thermomiotic and volumetric effects are found in ReO_3-perovskite family compounds, e.g. zero thermal expansion was reported for TaO_2F [12], variable thermal expansion was found for $Sc_{1-x}Y_xF_3$ [8], $Sc_{1-x}Ti_xF_3$ [13,14] and $Sc_{1-x}Al_xF_3$ [15] as a function of composition, as well as anomalously low-temperature heat capacity was reported for ScF_3–YF_3 solid solutions in Ref. 16. Simple and efficient production routes

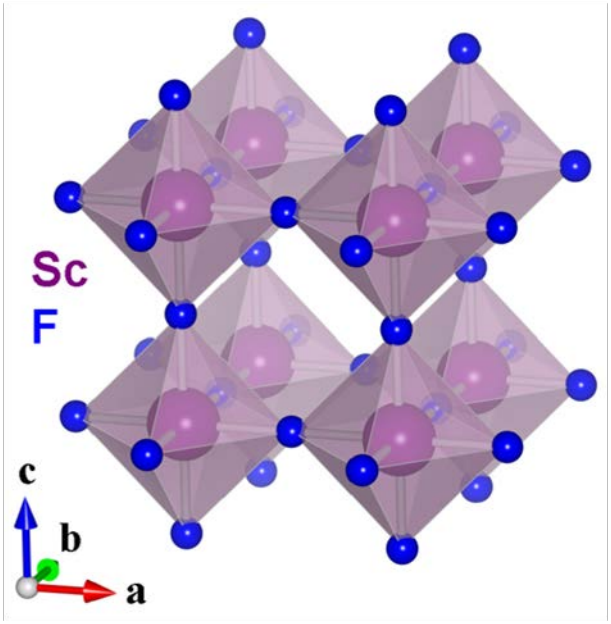

Fig. 1. Schematic view of cubic ScF_3 structure (space group *Pm*-3*m* (221)) built up of ScF_6 regular octahedra joined by corners (small balls are fluorine atoms, large balls are scandium atoms). All Sc–F –Sc angles are equal to 180°.

of ScF_3 were developed using hydrothermal method [17] and molten salt synthesis [18]. Recently metal fluorides were mentioned as a new class of NTE functional materials [19] with controllable thermal expansion by chemical modifications [20].

A cubic-to-rhombohedral phase transition occurs in ScF_3 at high pressure ($P > 0.5$ GPa at $T = 300$ K or $P = 0.1$–0.2 GPa at 50 K) as determined from x-ray and neutron diffraction studies [1,21]. Raman spectroscopy confirms that upon pressure increase cubic ScF_3 undergo a phase transition to the rhombohedral (space group *Rm*-3*c*) phase [21,22].

The electronic structure of ScF_3 thin films was experimentally investigated by resonant photoemission spectroscopy at the Sc 2*p* and F 1*s* absorption edges in Ref. 5. Two charge transfer-type satellites, the first one at about 13 eV below the main peaks in the valence-band and the second one with an energy separation of about 9–10 eV, were observed and indicate the strong hybridization effect between Sc 3*d* and F 2*p* states [5]. Electronic structure, magnetism and tunable luminescence properties of ScF_3 nano/microcrystals activated by lanthanides trivalent ions (Tb^{3+}, Eu^{3+}, Yb^{3+}, Er^{3+}, Tm^{3+} and Ho^{3+}) were studied in Ref. 23. The first calculations of ScF_3 band structure performed using local density approximation (LDA) approach was also presented in Ref. 23. Three hybrid functionals B3LYP, PBE0 and HSE06 as well as GW approximation (G is the Green's function and W the screened Coulomb interaction) with plane-wave basis set were used in [24] to study the electronic structure of ScF_3, YF_3, and AlF_3 wide-band-gap insulators.

The phonon properties of ScF_3 were studied using a combination of inelastic neutron scattering experiment with *ab initio* local density approximation augmented plane wave calculations of lattice dynamics [25]. It was shown that a description of NTE within the quasi-harmonic approximation is not reliable in the case of ScF_3. The authors in [25] demonstrated that the *R*4+ mode (the one with the lowest energy at *R*-point of Brillouin zone (BZ)) has quartic potential and proposed the mechanism of NTE based on this anharmonicity. The transition between the ground state and the first excited state (~19 meV) of the *R*4+ mode was associated with experimentally observed phonon peak (~25 meV), which stiffens upon increasing temperature [25]. The analysis of NTE effect is often performed considering the behavior of Grüneisen parameter, which can be determined from first-principles calculations within, for example, local density approximation (LDA) [25] or general gradient approximation (GGA) [26]. *Ab initio* molecular dynamics calculations in NpT ensemble were used very recently in Ref. 27 to calculate directly temperature dependence of the average ScF_3 lattice constant and to estimate its NTE effect.

In this study we report the results of *ab initio* band structure calculations for cubic ScF_3 using the linear combination of atomic orbital (LCAO) and plane wave projector augmented-wave (PAW) methods.

Computational details

Cubic ScF_3 was modelled using two methods: LCAO within the framework of hybrid density functional approach and PAW calculations using the generalized gradient approximation density functional.

To perform hybrid LCAO calculations, we used the periodic CRYSTAL09 code [28], which employs Gaussian-type functions centred on atomic nuclei as the basis set for expansion of the crystalline orbitals. The full-electron basis sets used in this study for F and Sc were taken from CRYSTAL basis set library [28]. Threshold parameters for evaluation of different types of bielectronic integrals such as overlap and penetration tolerances for Coulomb integrals, overlap tolerance for exchange integrals and pseudo-overlap tolerances for exchange integral series [28] have been set to 10^{-8}, 10^{-8}, 10^{-8}, 10^{-8} and 10^{-16}, respectively. Calculations are considered as converged when the total energy obtained in the self-consistent field procedure differs by less than 10^{-10} a.u. in the two successive cycles.

LCAO calculations of ScF_3 were performed using a set of hybrid Hartree–Fock/Kohn–Sham (HF/KS) exchange-correlation functionals [29–33] combining exact HF nonlocal exchange and KS exchange operator within the GGA as implemented in the CRYSTAL09 code [13]. We employed the following hybrid functionals: "BECKE & LYP", "BECKE & PWGGA", "PBE & PBE", "PBEsol & PBEsol", where the first terms refer to the KS exchange and the second terms to the KS correlation parts of a hybrid functional. The weight of the HF exchange was varied for each functional separately between 0 and 100%. ScF_3 full-electron basis set used in the calculations has even number of electrons ($21 + 3\times9 = 48$) therefore restricted Hartree–Fock scheme was used.

DFT calculations using the PAW method as implemented in the VASP code [34] were performed for comparison. We compared PW91 [33] and PBE [29] exchange-correlation potentials as well as large-core effective core potential (LC–ECP) with three $3d^1 4s^2$ valence electrons and small-core effective core potential (SC–ECP) with eleven $3s^2 3p^6 3d^1 4s^2$ valence electrons for Sc atom. Fluorine atom for all calculations was described as ECP with $2s^2 2p^5$ valence shell. Hybrid HF–DFT calculations were also performed with the weight of exact HF exchange part equal to 25%. The optimal cut-off energy was equal to 1000 eV. To provide the balanced summation over the direct and reciprocal lattices of ScF_3 in both LCAO and PAW methods, the reciprocal space integration was performed by sampling the BZ with the 8×8×8 Pack-Monkhorst *k*-mesh [35] that results in 35 eventually distributed *k*-points in the irreducible BZ.

Choice of exchange-correlation functional

The influence of the exchange-correlation functional type and the weight (*w*HF) of exact HF nonlocal exchange

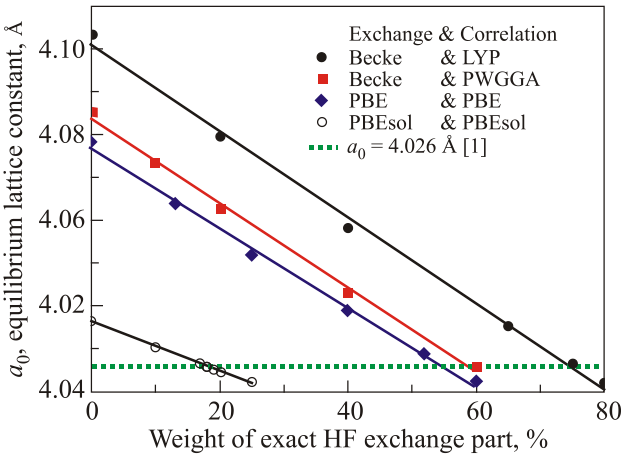

Fig. 2. (Color online) Dependence of the equilibrium lattice constant on the weight of exact HF non-local exchange in hybrid density calculation by the LCAO method.

in hybrid density calculations within the LCAO method on the lattice parameter in ScF_3 is shown in Fig. 2. We found that pure GGA functionals overestimate the experimental value of a_0 = 4.026 Å [1], while stepwise increase of the *w*HF for about 10% leads to proportional decrease of the lattice constant a_0 by approximately 0.01 Å. The PBEsol functional with *w*HF = 18% reproduces perfectly the experimental value of the lattice constant and was selected for further calculations.

Values of the lattice constant a_0 obtained using pure GGA calculations by the VASP code [34] are in the range of 4.02–4.03 Å when LC–ECP is used for Sc, while they are equal to 4.06–4.07 Å when SC–ECP was adopted for Sc. Using hybrid HF–DFT calculations with the PBE0 functional [34], the value of a_0 is equal to 4.04–4.05 Å, thus being between the results of LC–ECP and SC–ECP cases.

To additionally justify the choice of hybrid functional, we calculated the value of the band gap (E_g). Until now the band gap of ScF_3 was not precisely measured experimentally, but it is estimated to be larger than 7–8 eV [5]. All hybrid functionals constructed for LCAO method (*w*HF corresponds to a_0 = 4.026 Å, see Fig. 2) suggest that ScF_3 is an insulator with relatively large band gap E_g > 8 eV. In the PAW GGA calculations the band gap is underestimated as it is predicted by the theory for pure GGA functionals: it is equal to 5.5–6.0 eV. Hybrid PAW calculations allowed us to obtain E_g equal to 8–9 eV, which is closer to the experimental estimate. Thus, for band structure calculations we have finally chosen the "PBEsol & PBEsol" functional with *w*HF = 18%, giving E_g = 9.8 eV, for LCAO method and the PW91 functional with *w*HF = 25%, giving E_g = 8.9 eV, for PAW method. These results are in good agreement with other theoretical calculations. Note that non-hybrid LDA or GGA approaches tend to underestimate the band gap value of cubic ScF_3 (E_g = 6.075 eV in Ref. 23 and E_g = 6 eV in Ref. 25). In turn the use of hybrid functional allows to obtain the band gap values in the range of 8.79–9.59 eV [24].

Electronic properties

The effective charges of scandium and fluorine atoms were calculated using Mulliken population analysis [28] in LCAO method and Bader topological analysis [36] in PAW calculations. The LCAO charges are equal to q_{Sc} = +2.28*e* and q_F = −0.76*e*. In PAW method the atom charges were slightly different for two Sc pseudopotentials: q_{Sc} = +2.70*e* and q_F = −0.90*e* for LC–ECP and q_{Sc} = +2.17*e* and q_F = −0.73*e* for SC–ECP. These results

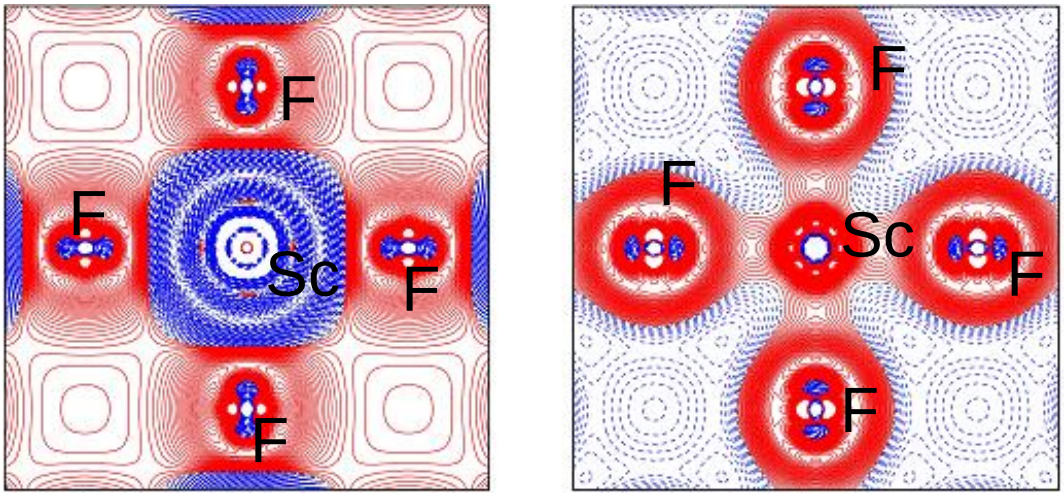

Fig. 3. (Color online) Plots of the charge density difference in (100) plane of ScF_3 between the full charge density of the crystal and electronic density of non-interacting atoms (left panel) and ions (right panel) obtained using "PBEsol & PBEsol" functional with *w*HF = 18%. Solid (red) and dashed (blue) isolines correspond to positive (excess) and negative (deficiency) electron density difference, respectively.

demonstrate a considerable deviation of effective atomic charges from formal charges caused by partly covalent nature of Sc–F bonds.

Figure 3 shows electron density maps in (100) plane of ScF_3 obtained using LCAO calculation as a difference between the full charge density of crystal and electronic density of non-interacting atoms or ions. The anisotropy of electron density induced by bond covalent contribution is clearly visible in both graphs: the electron density is larger along the crystallographic axes. In Fig. 4 we compare the partial F *p* density of states (DOS) calculated by both LCAO and PAW methods with the experimental valence-band (VB) photoelectron spectrum taken from Ref. 37 and the F 1*s* x-ray absorption spectrum taken from Ref. 5. The VB photoelectron spectrum of ScF_3 has a complex shape composed of the main peak and the shoulder located at the left side, which originate due to the valence band splitting upon hybridization of the F 2*p* and Sc 3*d* states [37]. Our theoretical calculations confirm such interpretation and reproduce well the width and asymmetric shape of the valence band. The F 1*s* absorption spectrum [5] consists of three well visible peaks at 9.3, 11.4 and 18.2 eV due to transitions from the F 1*s* core state to the F *np* states in the conduction band and above. The first two peaks correspond to the F 2*p* states in the conduction band, which are hybridized with the Sc 3*d* states. The two peaks originate from the t_{2g}-e_g splitting of the Sc 3*d* states by the octahedral crystal field. The third peak at 18.2 eV corresponds to the interaction of the F 2*p* and Sc 4*p* states. Such interpretation is fully supported by the calculated F *p* DOS: in fact, good agreement with the F 1*s* absorption spectrum indicates that a relaxation of the electron states due to the F 1*s* core-hole is weak in ScF_3.

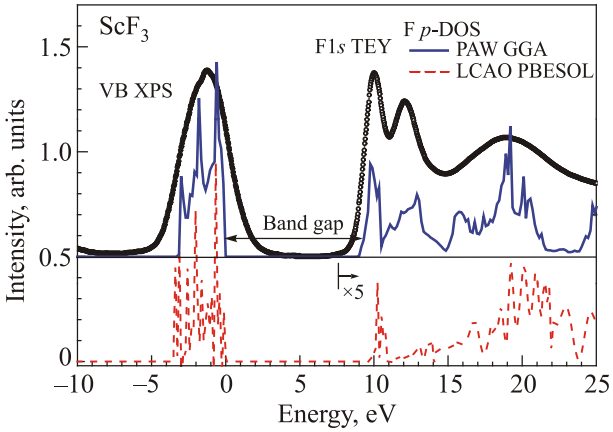

Fig. 4. (Color online) A comparison of the F *p* density of states (DOS) calculated by means of the LCAO (dashed line) and PAW (solid line) methods with valence-band photoelectron [37] and F 1*s* x-ray absorption spectra [5]. The amplitude of the DOS in the conduction band was multiplied by a factor of 5. Energy scale is given with respect to the calculated top of the valence band. Experimental spectra have been aligned to match best the calculations.

The analysis of band structures for ScF_3 bulk presented in Fig. 5 calculated by LCAO and PAW methods demonstrates even good quantitative correlation between both methods. The analysis of the band structure suggests that the band gap in ScF_3 is indirect. However, in contrast to Han *et al.* [23], who found the indirect XR transition, our

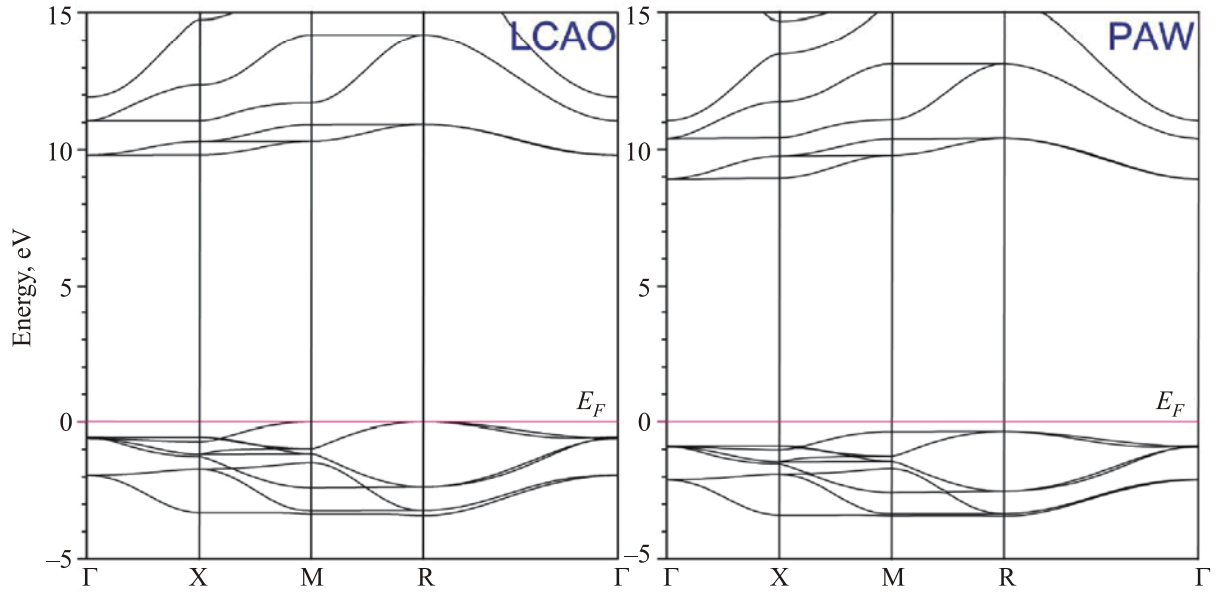

Fig. 5. The energy bands of ScF_3 crystal constructed for LCAO calculations with PBEsol & PBEsol functional and weight of exact HF nonlocal exchange *w*HF = 18% (full-electron basis set, left panel) and PAW calculation with PW91 functional and *w*HF = 25% (LC–ECP, right panel). The energies are given in eV, Fermi level E_F is shown with horizontal magenta line.

calculation shows that the indirect band gap is between the top of the valence band (VB) at the R point and the bottom of the conduction band (CB) at the Γ point of the BZ. These results are in agreement with results presented by Hamed *et al.* in [24] where indirect band gap E_g with R–Γ transition was also found (E_g = 9.59 eV for Hybrid–PBE [29], 8.79 eV for Hybrid–HSE06 [38] and 8.89 eV for Hybrid–B3LYP [31] potentials). These results show the importance of hybrid functional use for electronic structure calculations in such systems as ScF_3.

Conclusions

The lattice constant, band gap and electronic properties of cubic ScF_3 were calculated using LCAO and plane wave PAW DFT computational methods. It was shown that a variation of exact HF exchange part allowed us to reproduce experimental value of the lattice constant a_0 = 4.026 Å [1].

The band gap obtained in hybrid HF–DFT calculations is equal to 8–10 eV and agrees well with the expected experimental value [5] and other hybrid calculations [24]. A deviation of atom charges from formal ones and anisotropy of electronic density point to the covalent nature of Sc–F bonds in ScF_3. Calculated partial F *p* DOS is in good agreement with valence-band photoelectron [37] and F 1*s* x-ray absorption [5] spectra.

Good agreement between the theory and available experimental data makes promising the application of the present approach to the investigation of phonon properties in ScF_3 in the future work.

Acknowledgments

Authors are greatly indebted to R.A. Evarestov, D. Gryaznov, V. Kashcheyevs, M. Krack, V. Pankratov, A.I. Popov, L. Shirmane, and Yu.F. Zhukovskii for many stimulating discussions. Financial support provided by Scientific Research Project for Students and Young Researchers Nr. SJZ2015/6 realized at the Institute of Solid State Physics, University of Latvia is greatly acknowledged.

1. B.K. Greve, K.L. Martin, P.L. Lee, P.J. Chupas, K.W. Chapman, and A.P. Wilkinson, *J. Am. Chem. Soc.* **132**, 15496 (2010).
2. T. Chatterji, P.F. Henry, R. Mittal, and S.L. Chaplot, *Phys. Rev. B* **78**, 134105 (2008).
3. E.E. Rodriguez, A. Llobet, T. Proffen, B.C. Melot, R. Seshadri, P.B. Littlewood, and A.K. Cheetham, *J. Appl. Phys.* **105**, 114901 (2009).
4. J. Purans, P. Fornasini, S.E. Ali, G. Dalba, A. Kuzmin, and F. Rocca, *Phys. Rev. B* **92**, 014302 (2015).
5. M. Umeda, Y. Tezuka, S. Shin, and A. Yagishita, *Phys. Rev. B* **53**, 1783 (1996).
6. J.S.O. Evans, *J. Chem. Soc., Dalton Trans.* **19**, 3317 (1999).
7. G.D. Barrera, J.A.O. Bruno, T.H.K. Barron, and N.L. Allan, *J. Phys.: Condens. Matter* **17**, R217 (2005).
8. C.R. Morelock, B. K. Greve, L.C. Gallington, K.W. Chapman, and A.P. Wilkinson, *J. Appl. Phys.* **114**, 213501 (2013).
9. A. Antuzevics, U. Rogulis, A. Fedotovs, Dz. Berzins, V.N. Voronov, and J. Purans, *Phys. Scr.* **90**, 115801 (2015).
10. S.U. Handunkanda, E.B. Curry, V. Voronov, A.H. Said, G.G. Guzmán-Verri, R.T. Brierley, P.B. Littlewood, and J.N. Hancock, *Phys. Rev. B* **92**, 134101 (2015).
11. C.R. Morelock, M.R. Suchomel, and A.P. Wilkinson, *J. Appl. Cryst.* **46**, 823 (2013).
12. C.R. Morelock, B.K. Greve, M. Cetinkol, K.W. Chapman, P.J. Chupas, and A.P. Wilkinson, *Chem. Mater.* **25**, 1900 (2013).
13. C.R. Morelock, L.C. Gallington, and A. P. Wilkinson, *Chem. Mater.* **26**, 1936 (2014).
14. L. Wang, C. Wang, Y. Sun, S. Deng, K. Shi, H. Lu, P. Hu, and X. Zhang, *J. Am. Ceram. Soc.* **98**, 2852 (2015).
15. C.R. Morelock, L.C. Gallington, and A.P. Wilkinson, *J. Solid. State. Chem.* **222**, 96 (2015).
16. C.P. Romao, C.R. Morelock, M.B. Johnson, J.W. Zwanziger, A.P. Wilkinson, and M.A. White, *J. Mater. Sci.* **50**, 3409 (2015).
17. L. Hu, J. Chen, Z. Pan, J. Deng, R. Yu, and X. Xing, *J. Am. Ceram. Soc.* **97**, 1386 (2014).
18. L. Hu, J. Chen, L. Fan, J. Deng, R. Yu, and X. Xing, *J. Am. Ceram. Soc.* **97**, 1009 (2014).
19. L. Wang, C. Wang, Y. Sun, K. Shi, S. Deng, H. Lu, P. Hu, and X. Zhang, *J. Materiomics* **1**, 106 (2015).
20. J. Chen, L. Hu, J. Denga, and X. Xing, *Chem. Soc. Rev.* **44**, 3522 (2015).
21. K.S. Aleksandrov, N.V. Voronov, A.N. Vtyurin, A.S. Krylov, M.S. Molokeev, A.S. Oreshonkov, S.V. Goryainov, A.Yu. Likhacheva, and A.I. Ancharov, *Phys. Solid State* **53**, 564 (2011).
22. K.S. Aleksandrov, N.V. Voronov, A.N. Vtyurin, S.V. Goryainov, N.G. Zamkova, V.I. Zinenko, and A.S. Krylov, *J. Exper. Theor. Phys.* **94**, 977 (2002).
23. L. Han, Y. Wang, L. Guo, L. Zhao, and Y. Tao, *Nanoscale* **6**, 5907 (2014).
24. H.B. Hamed, A. Qteish, N. Meskini, and M. Alouani, *Phys. Rev. B* **92**, 165202 (2015).
25. C.W. Li, X. Tang, J.A. Muñoz, J.B. Keith, S.J. Tracy, D.L. Abernathy, and B. Fultz, *Phys. Rev. Lett.* **107**, 195504 (2011).
26. Y. Liu, Z. Wang, M. Wu, Q. Sun, M. Chao, and Y. Jia, *Comp. Mater. Sci.* **107**, 157 (2015).
27. P. Lazar, T. Bučko, and J. Hafner, *Phys. Rev. B* **92**, 224302 (2015).
28. R. Dovesi, V.R. Saunders, C. Roetti, R. Orlando, C.M. Zicovich-Wilson, F. Pascale, B. Civalleri, K. Doll, N.M. Harrison, I.J. Bush, Ph. D'Arco, and M. Llunell, *CRYSTAL09 User's Manual*, University of Torino, Torino (2009).
29. J.P. Perdew, K. Burke, and M. Ernzerhof, *Phys. Rev. Lett.* **77**, 3865 (1996).

30. J.P. Perdew, A. Ruzsinszky, G.I. Csonka, O.A. Vydrov, G.E. Scuseria, L.A. Constantin, X. Zhou, and K. Burke, *Phys. Rev. Lett.* **100**, 136406 (2008).
31. C. Lee, W. Yang, and R.G. Parr, *Phys. Rev. B* **37**, 785 (1988).
32. A.D. Becke, *Phys. Rev. A* **38**, 3098 (1988).
33. J.P. Perdew, J.A. Chevary, S.H. Vosko, K.A. Jackson, M.R. Pederson, D.J. Singh, and C. Fiolhais, *Phys. Rev. B* **46**, 6671 (1992).
34. G. Kresse, M. Marsman, and J. Furthmüller, *VASP the GUIDE*, University of Wien, Wien (2012).
35. H.J. Monkhorst, and J.D. Pack, *Phys. Rev. B* **13**, 5188 (1976).
36. R.F.W. Bader, *Atoms in Molecules, A Quantum Theory*, Oxford University Press, Oxford (1990).
37. S. Shin, Y. Tezuka, T. Ishii, and Y. Ueda, *Solid State Commun.* **87**, 1051 (1993).
38. A.V. Krukau, O.A. Vydrov, A.F. Izmaylov, and G.E. Scuseria, *J. Chem. Phys.* **125**, 224106 (2006).